PCCP

Accepted Manuscript

This article can be cited before page numbers have been issued, to do this please use: D. Velasco Castrillo, M. Reig and J. Puigdollers, *Phys. Chem. Chem. Phys.*, 2017, DOI: 10.1039/C7CP05135B.

ROYAL SOCIETY OF CHEMISTRY

rsc.li/pccp

View Article Online
DOI: 10.1039/C7CP05135B

Journal Name

ARTICLE

Solid-state organization of n-type carbazole-based semiconductors for organic thin-film transistors

Received 00th January 20xx,
Accepted 00th January 20xx

DOI: 10.1039/x0xx00000x

www.rsc.org/

Marta Reig,[a] Joaquim Puigdollers[b] and Dolores Velasco*[a]

The development of new organic semiconductors has been mainly led by the search of new π-conjugated cores, but recently the use of flexible side chains is attracting more and more attention to control the molecular packing and order in the solid state to improve the charge-transporting properties. In this work, the charge transport properties of a series of tricyanovinyl-substituted carbazole-based materials with different alkyl chain length have been investigated and correlated with the respective intermolecular interactions and molecular packing via X-ray diffraction (XRD) studies.

Introduction

Organic semiconductors have received significant attention as active layers in organic thin-film transistors (OTFTs),[1] organic light-emitting diodes (OLEDs)[2] and organic solar cells,[3] due to their attractive properties such as low cost, capability of covering large-area and flexible devices, and above all, the possibility to easily tune their electronic and optoelectronic properties by means of the molecular design.

Particularly, the development of OTFT active materials has improved considerably during the last decades, but to date n-type semiconductors have been less developed than their p-type counterparts. Considering that both p- and n-type semiconductors are required for ambipolar transistors and organic complementary circuits, many efforts are still focused on the development of n-type materials with enhanced performance.[4]

From the chemical design point of view, several considerations should be taken into account to obtain n-type semiconducting materials with high charge carrier mobilities and stability under ambient conditions. Firstly, independently of the kind of charge carriers, holes or electrons, large conjugated π-systems favour π–π stacking intermolecular interactions and maximize the electronic coupling between adjacent molecules.[5,6] Secondly, the attachment of electron acceptor groups on the conjugated π-system potentially affords n-type materials with high enough electron affinity (EA) to allow efficient charge injection.[5,6] Finally, the introduction of flexible side chains in the π-conjugated core impacts on the film-forming properties of the organic semiconductor and could play an important role in the charge-transporting properties.[7] Since the conjugated π-electron system is the responsible for the inherent electronic and optoelectronic properties of the organic semiconductor material, many research is directed to the development of new π-conjugated cores,[6,8] but less attention has been paid to the role that play the flexible side chains, which are usually used as solubilizing groups for easy handling of the materials. However, besides providing better solubility, the introduction of side chains (*i.e.* alkyl chains) has emerged as an effective strategy to control the molecular packing of the organic semiconductors in the solid state.[7,9]

Recently, we have reported the charge-transporting properties of a series of push-pull derivatives based on the electron-donating carbazole and the electron-withdrawing tricyanovinyl groups.[10] The π-conjugated carbazole heterocycle is recognised as a suitable building block in organic electronics, because of its low cost and easy availability, easy chemical functionalization, high thermal and chemical stability, high photoluminescence quantum yields and excellent hole-transporting properties.[11] Remarkably, by only a single synthetic step, the tricyanovinyl group can be easily attached to position 3 of the carbazole core furnishing materials with high EA (> 4 eV) that plays a crucial role on the charge-transporting properties. In this way, n-channel conduction can be observed instead of the characteristic p-type behaviour of carbazole derivatives.[10]

This work involves a series of tricyanovinyl-substituted carbazole-based materials that differ only in the length of the *N*-alkyl chain of the carbazole moiety. Hence, the dependence of the charge carrier mobilities on the *N*-alkyl chain length is reported herein. The charge-transporting properties were

[a] Grup de Materials Orgànics, Institut de Nanociència i Nanotecnologia (IN²UB), Departament de Química Inorgànica i Orgànica, Secció de Química Orgànica, Universitat de Barcelona, Martí i Franquès 1, E-08028, Barcelona, Spain. E-mail: dvelasco@ub.edu; Fax: +34 93 339 78 78; Tel: +34 93 403 92 60
[b] Dept. Enginyeria Electrònica, Universitat Politècnica de Catalunya, C/ Jordi Girona 1-3, E-08034, Barcelona, Spain.

† Footnotes relating to the title and/or authors should appear here.
Electronic Supplementary Information (ESI) available: Crystallographic data, TGA and DSC curves, cyclic voltammograms, OTFT characteristics, powder XRD spectra. See DOI: 10.1039/x0xx00000x

View Article Online
DOI: 10.1039/C7CP05135B

determined by the measurement of OTFT devices. In addition, the molecular structure of the organic materials has been examined by X-ray diffraction (XRD) studies.

Results and discussion

Synthesis

The synthesis of 9-alkyl-3-(1,2,2)-tricyanovinyl)-9*H*-carbazole derivatives **1–5** is shown in Scheme 1. The selected alkyl chain lengths have been of 1, 2, 4, 8 and 12 carbon units to generate the corresponding **1–5** derivatives, respectively. Compounds **1–5** were easily prepared by heating the corresponding *N*-alkylated carbazole precursor in the presence of tetracyanoethylene in anhydrous *N*,*N*-dimethylformamide (DMF) at 50 °C.[12] Previously, *N*-alkyl derivatives were obtained by alkylation[13–15] of 9*H*-carbazole using NaH as a base in DMF in high yields. Derivatives **1**,[10,16] **2**[16,17] and **3**[16] have been previously described in the literature. All compounds were fully characterized by ^{1}H NMR and ^{13}C NMR spectroscopies and mass spectrometry.

Thermal, optical and electrochemical properties

Thermal properties of this series of compounds were analysed by thermogravimetric analysis (TGA) and differential scanning calorimetry (DSC). The thermal characteristics of compounds **1–5** are summarized in Table 1, and TGA and DSC curves can be found in Fig. S1–S2† in the ESI. All compounds possess high thermal stabilities, with decomposition temperatures (T_d) higher than 296 °C. DSC thermograms of compounds **1–5** show a melting process during the first heating scan together with an exothermic peak during the cooling scan attributed to the crystallization process. The melting point decreases considerably as the alkyl chain length increases, as it is shown from the *N*-methyl derivative **1** (T_m = 245 °C) to the *N*-dodecyl counterpart **5** (T_m = 136 °C).

UV-vis absorption spectra of compounds **1–5** in dichloromethane solutions and in thin films show two absorption regions that cover the UV and the visible electromagnetic spectrum (Table 1 and Fig. 1). The first absorption region, which is attributed to the carbazole unit, is located in the UV zone with a maximum at 290–292 nm in solution. The second broad absorption band is centred at lower energy (490–494 nm in solution) and attributed to the intramolecular charge transfer from the electron-donating carbazole moiety to the electron-withdrawing tricyanovinyl group.[10] In solution, all compounds display practically identical absorption spectra independently of the *N*-alkyl substitution of

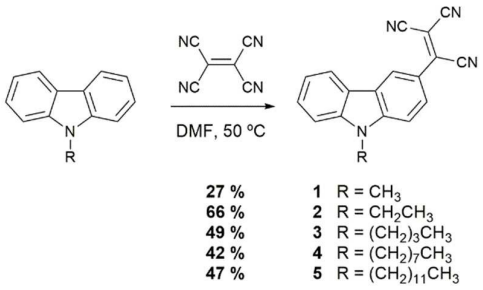

Scheme 1 Synthesis of tricyanovinyl-substituted derivatives **1–5**.

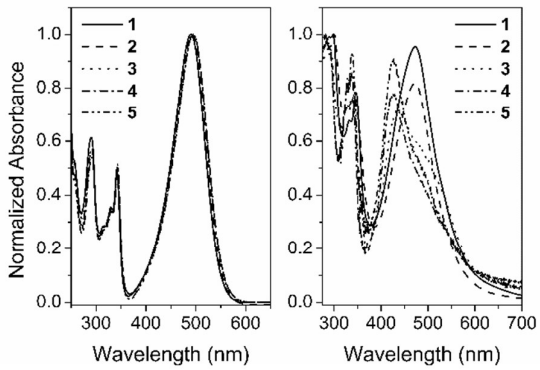

Fig. 1 UV-vis absorption spectra of compounds **1–5** of a) 10 μM dichloromethane solutions and b) vacuum-evaporated thin films of 75 nm.

Table 1 Thermal, optical and electrochemical properties of carbazole derivatives **1–5**.

Compound	T_d [a] (°C)	T_m [b] (°C)	T_c [b] (°C)	$\lambda_{abs,max}$ (nm) [c] [ε (dm^3 mol^{-1} cm^{-1})]	$\lambda_{abs,max}$ [d] (nm)	$E^0_{red,1}$ [e] (V)	E^{red}_{onset} [f] (V)	E^{ox}_{onset} [f] (V)	EA [g] (eV)	IP [g] (eV)	E_{gap} [g] (eV)
1 [h]	301	245	231	290 (19 667), 490 (32 090)	298, 472	–1.08	–1.00	1.06	4.39	6.45	2.06
2	296	243	214	292 (13 018), 493 (22 860)	300, 472	–1.08	–1.00	1.07	4.39	6.46	2.07
3	304	168	131	292 (12 168), 494 (21 858)	282, 436	–1.08	–1.00	1.06	4.39	6.45	2.06
4	319	147	110	292 (13 641), 494 (25 256)	282, 425	–1.08	–1.00	1.07	4.39	6.46	2.07
5	326	136	105	292 (13 534), 494 (23 595)	283, 427	–1.08	–1.00	1.07	4.39	6.46	2.07

[a] Onset decomposition temperature (T_d) obtained from TGA performed at a heating rate of 20 °C min^{-1}. [b] Melting point (T_m) and crystallization temperature (T_c) obtained from DSC performed at a scan rate of 10 °C min^{-1}. [c] Measured in 10 μM dichloromethane solutions at room temperature. [d] Measured in vacuum-evaporated thin films (75 nm) on quartz substrates at room temperature. [e] Standard potential of the first reduction redox couple ($E^0_{red,1}$) *vs.* Fc$^+$/Fc estimated from cyclic voltammetries of 1 mM dichloromethane solutions at a scan rate of 100 mV s^{-1}. [f] Onset reduction potential (E^{ox}_{onset}) and onset oxidation potential (E^{red}_{onset}) *vs.* Fc$^+$/Fc estimated from cyclic voltammetries of 1 mM dichloromethane solutions at a scan rate of 100 mV s^{-1}. [g] Estimated from cyclic voltammetries as EA = $E^{red}_{onset\ vs.\ Fc^+/Fc}$ + 5.39, IP = $E^{ox}_{onset\ vs.\ Fc^+/Fc}$ + 5.39, and E_{gap} = IP – EA. [h] Data taken from Ref. 10.

View Article Online
DOI: 10.1039/C7CP05135B

the carbazole moiety. However, some information can be obtained by comparing the absorption spectra in solution and in the solid state. The absorption spectra of thin films show an hypsochromic shift of the maximum of the charge-transfer absorption band in comparison to that observed in solution. The hypsochromic shift is more significant as the *N*-alkyl chain length increases, as revealed by compounds **1** (18 nm), **2** (21 nm), **3** (58 nm), **4** (69 nm) and **5** (67 nm). These results are indicative of the influence of the *N*-alkyl chain length on the molecular packing in the solid state, which will be discussed below through the single-crystal X-ray analysis.

The electrochemical properties of compounds **1**–**5** were characterized by cyclic voltammetry (Table 1). All compounds display identical redox behaviour as the previously reported for derivative **1**.[10] Cyclic voltammograms exhibit two reduction waves, being the first one *quasi*-reversible and the second one irreversible, together with one irreversible oxidation wave (Fig. S3† in the ESI). Electron affinities (EA) and ionization potentials (IP) of this series of compounds were estimated to be 4.39 and 6.45–6.46 eV, respectively. The high EA values of these compounds are indicative of their potential n-type properties.

Single-crystal X-ray analyses

The crystal structures of compounds **2**–**5** were determined by single-crystal X-ray analysis. Suitable single crystals were grown by slow evaporation from the corresponding dichloromethane (**2**), chloroform (**3**) and acetone (**4** and **5**) solutions. For compound **1**, two different crystalline structures have been reported.[10,18] The detailed crystallographic data of **2**–**5** can be found in Table S1–S4† in the ESI. Molecules **1**–**5** adopt an almost planar conformation independently of the length of the *N*-alkyl chain (Fig. S4† in the ESI).

The crystal structures of **1**–**5** derivatives show a layered organization with an antiparallel arrangement (Fig. 2 and 3). All compounds show π–π stacking interactions with similar minimum interlayer distances of 3.28–3.40 Å. This molecular arrangement and the planar conformation of the molecules favour LUMO-LUMO interactions, contributing in the enhancement of the electron transport.[10] Remarkably, the length of the *N*-alkyl chain is crucial in determining the molecular packing motif in the solid state. Thus, molecules with the shorter *N*-alkyl chains, methyl to butyl, adopt a herringbone structure through C–H···π and C–H···NC hydrogen bonding intermolecular interactions established among adjacent π-stacks (Fig. 2). In contrast, the introduction of the longer alkyl chains, octyl and dodecyl, in **4** and **5** inhibits the possibility of such interactions along one of the axis whereas they can be maintained through the others one. Consequently, molecules of adjacent π stacked arrays separated by the insulating interdigitated alkyl chains are induced to adopt a coplanar arrangement (Fig. 3).

Organic Thin-Film Transistors

Charge-transporting properties of compounds **1**–**5** were studied in bottom-gate/top-contact OTFTs by using polystyrene (PS) treated c-Si/SiO_2 gate/dielectric substrates and Au as source and drain electrodes. The semiconductor thin films were deposited by the thermal vacuum evaporation technique (with a base pressure below 10^{-6} mbar).

Devices based on **1**–**5** showed typical characteristics of n-type transistors (Table 2, Fig. 4 and Fig. S5–S9† in the ESI). The electrical characterization of OTFTs has been performed in vacuum in order to prevent the degradation of the devices. OTFT devices with PS-treated substrates based on compounds **1**–**5** exhibited similar electron mobilities in the range of 9×10^{-6} to 5×10^{-5} cm^2 V^{-1} s^{-1}, according to the comparable

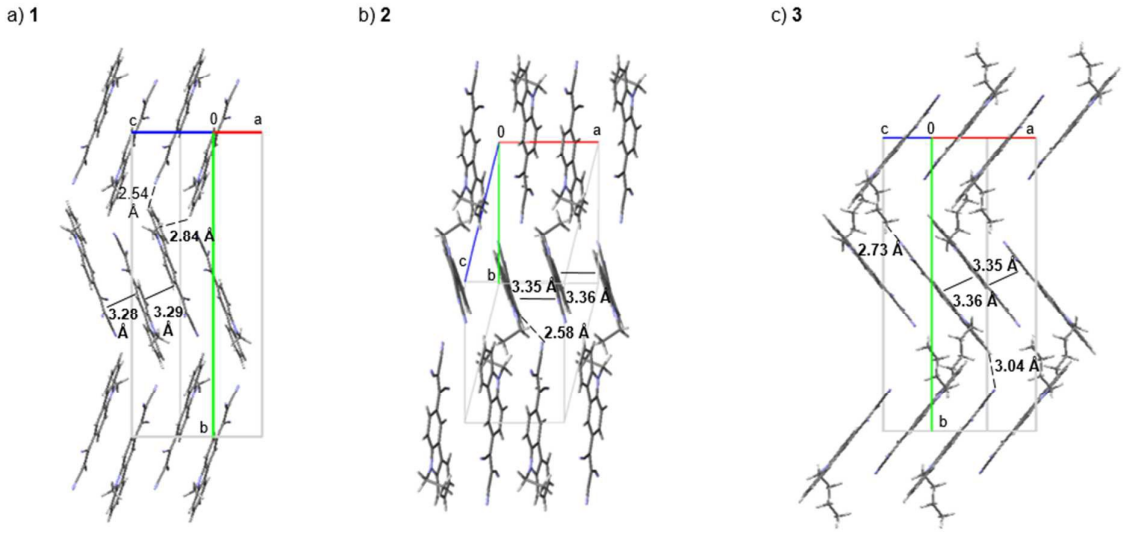

Fig. 2 Crystal structures of a) **1**, b) **2** and c) **3**.

View Article Online
DOI: 10.1039/C7CP05135B

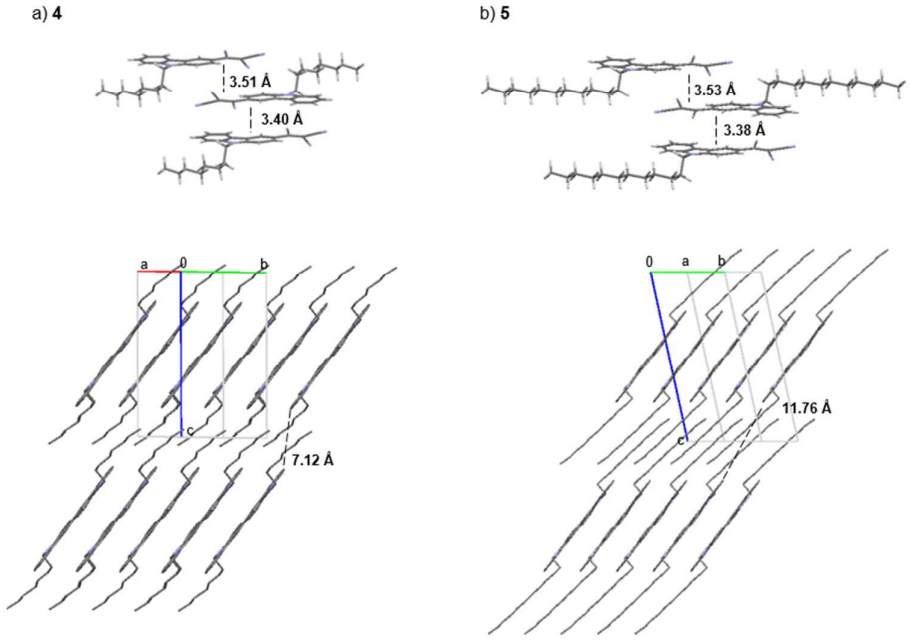

Fig. 3 Crystal structures of a) **4** and b) **5**. Hydrogen atoms have been removed for clarity in the representation of the molecular packing.

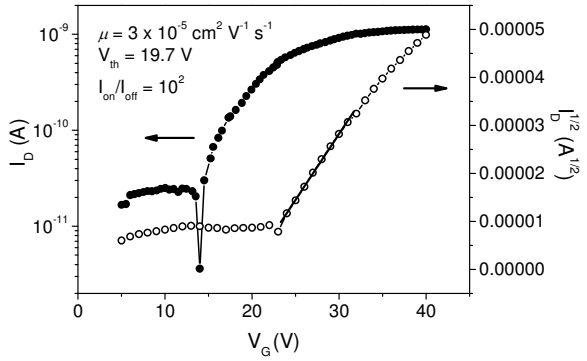

Fig. 4 Transfer (V_D = 10 V) and saturation characteristics of an OTFT device fabricated with compound **1** as the semiconductor layer and with PS-treated substrate.

Table 2 OTFT characteristics of devices based on tricyanovinyl-substituted carbazole derivatives **1–5** with PS and OTS-treated c-Si/SiO_2 substrates.

Compd.		μ_e [a] ($cm^2 V^{-1} s^{-1}$)	V_{th} [b] (V)	I_{on}/I_{off} [c]
1	PS	3×10^{-5}	19.7	$\sim 10^2$
1	OTS	2×10^{-5}	23.6	$\sim 10^3$
2	PS	9×10^{-6}	25.6	$\sim 10^1$
3	PS	2×10^{-5}	15.3	$\sim 10^2$
4	PS	3×10^{-5}	19.6	$\sim 10^4$
5	PS	5×10^{-5}	19.6	$\sim 10^4$

[a] Electron mobility (μ_e). [b] Threshold voltage (V_{th}). [c] I_{on}/I_{off} ratio. OTFT measurements were determined in vacuum and at room temperature.

antiparallel arrangement in the π stacks with similar interlayer distances that all of them exhibit. Threshold voltages were also similar for all the prepared devices (15.3–25.6 V), but in contrast it can be mentioned that those devices based on the derivatives with the long alkyl chains, the *N*-octyl **4** and *N*-dodecyl **5** materials, showed the larger I_{on}/I_{off} ratios ($\sim 10^4$). In order to study the effect of the dielectric treatment on the device performance, an OTFT device with octadecyltrichlorosilane (OTS) treated c-Si/SiO_2 surface based on compound **1** was prepared. Similar electron mobilities were achieved for devices of **1** on PS- and OTS-treated substrates around 2–3 × 10^{-5} cm^2 V^{-1} s^{-1}. Given that no significant improvement was observed, no further OTFT devices with OTS-treated substrates were prepared for its analogues.

Molecular order and morphology of the OTFT active layers

In order to correlate the charge transport properties with the molecular structure in the thin films, vacuum-evaporated layers (75 nm) of **1** deposited on PS- and OTS-treated c-Si/SiO_2 substrates and of **2–5** deposited on PS-treated substrates were subjected to Grazing Incidence X-Ray Diffraction (GIXRD) and Atomic Force Microscopy (AFM) studies. Fig. 5 displays the GIXRD patterns of the above-mentioned layers of compounds **1–5**. It should be mentioned that the longer alkyl chains induce more ordered films. In fact, GIXRD spectra of layers of **1–3** show in general multiple weak diffraction peaks, whereas films of **4** and **5** show only one strong diffraction peak.

GIXRD spectrum of the film of **1** deposited on PS-treated c-Si/SiO_2 substrate shows several weak diffraction peaks at 2θ = 9.28°, 10.68° and 13.02°. Similarly, the GIXRD spectrum of the layer of **1** deposited on OTS-treated substrate shows the

View Article Online
DOI: 10.1039/C7CP05135B

diffraction peaks at 2θ = 9.22°, 10.72° and 13.02°. However, GIXRD spectra of **1** do not correspond neither to the powder XRD spectra nor to the single crystal data. Therefore, it was not possible to establish the molecular orientation in the films.

Layers of **2** prepared on PS-treated c-Si/SiO_2 substrates show several weak diffraction peaks and one strong diffraction peak at 2θ = 8.88°, which suggest a preferred orientation in the film. Combining the single crystal data and the powder XRD spectra, this stronger diffraction peak can be assigned to the reflection 011, indicating that the (011) plane is parallel to the c-Si/SiO_2 substrate, with the *a*-axis also in the parallel plane. In a similar way, the GIXRD spectrum of the layer of **3** on PS-treated substrate shows more than one diffraction peak. The strongest diffraction peak at 2θ = 7.28° can be attributed to the reflection 020, indicating that the (010) plane is parallel to the c-Si/SiO_2 substrate, with the *a*- and *c*-axis also in the parallel plane. The molecular packing in the thin films of **2** and **3** corresponds to that of the corresponding derivatives in the single crystals and as a result, it can be concluded that molecules in layers of **2** and **3** exhibit a preferred orientation as displayed in Fig. 2b and c with the π–π stacking direction being parallel to the substrate surface.

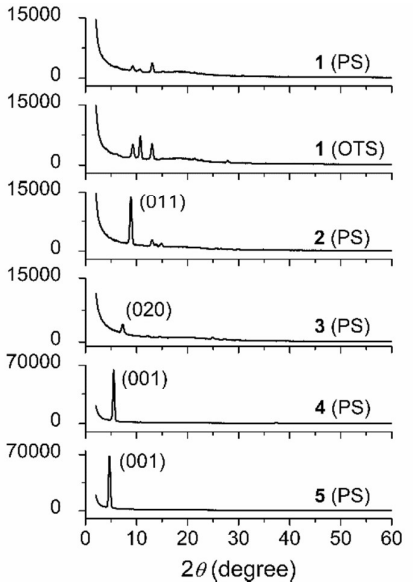

Fig. 5 GIXRD patterns of vacuum-deposited layers of **1** on PS- and OTS-treated c-Si/SiO_2 substrates and of **2–5** on PS-treated c-Si/SiO_2 substrates.

GIXRD spectra of thin films of compounds **4** and **5** show only one strong diffraction peak at 2θ = 5.52° and 4.68°, respectively, indicating that **4** and **5** form well-ordered films under the experimental conditions. Combining the single crystal data and the powder XRD spectra, the diffraction peaks at 2θ = 5.52° for **4** and 2θ = 4.68° for **5** can be assigned to the reflection 001, indicating that the (001) plane is parallel to the c-Si/SiO_2 substrate, *i.e.* with *a*- and *b*-axis also in the parallel plane. The XRD study indicates that the molecular packing in the thin films corresponds to that of the corresponding derivatives **4** and **5** in the single crystals. Molecules in films of **4** and **5** are oriented with the π–π stacking direction being parallel to the substrate surface as shown in Fig. 3 (below).

According to the XRD study, vacuum-evaporated layers of compounds **2–5** show a similar layered organization with the π–π stacking direction being parallel to the substrate surface. This kind of molecular organization is recognised to be appropriate for obtaining enhanced charge carrier mobilities in OTFTs. Therefore, this results justify that OTFTs with PS-treated substrates based on **2–5** show similar electron mobilities independently of the alkyl chain length.

Here, it should be highlighted that the distance between adjacent π stacks are significantly increased in compounds with longer alkyl chains **4** and **5** by the interdigitated alkyl chains, showing minimum distances of 7.12 and 11.76 Å, respectively (Fig. 3). Since these alkyl chains act as insulating parts and do not contribute to the charge transport process,[7] a

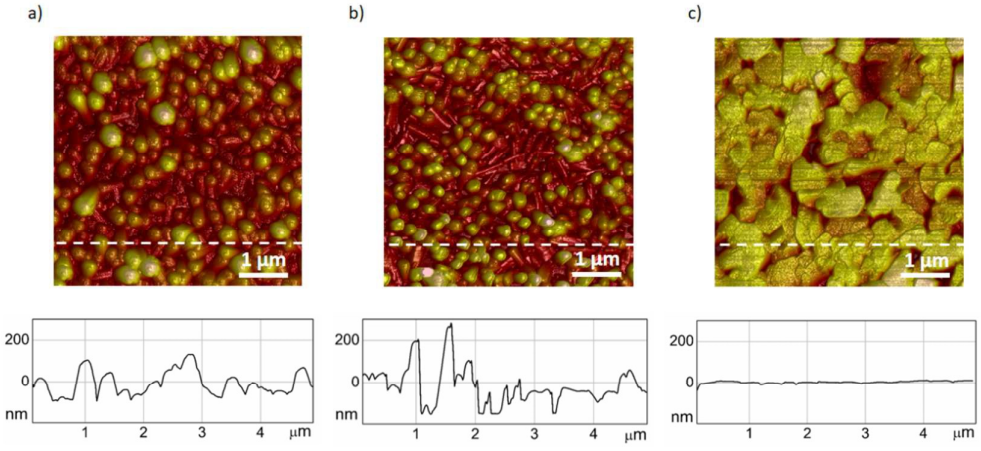

Fig. 6 AFM images (5 × 5 μm^2) of vacuum-evaporated thin films (above) and sections (below) of a) **1** on PS-treated SiO_2, b) **2** on PS-treated SiO_2 and c) **4** on PS-treated SiO_2.

View Article Online
DOI: 10.1039/C7CP05135B

worse device performance could be expected for **4** and **5** based devices. However, OTFTs based on this series of tricyanovinyl derivatives showed comparable electron mobilities, being the I_{on}/I_{off} ratios higher for those devices based on **4** and **5**. Thus, the use of long alkyl chains induces a higher degree of long range organization of the molecules in the film leading to OTFTs with enhanced device performance. This strategy resembles that previously reported, where block copolymers, consisting of electro-active conjugated rod blocks and non-conjugated flexible coil blocks, are investigated to create segregated domains to induce well-organized nanostructures, resulting in the enhancement of the charge-transporting properties.[7a,19]

The morphology of the films of **1–5** was studied by AFM to further investigate the film-forming properties of this series of derivatives. Fig. 6 collects the AFM images taken from vacuum-evaporated films of **1**, **2** and **4** on PS-treated c-Si/SiO_2 substrates. Layers of derivatives with the shorter alkyl chains **1** and **2** show continuous films with similar granular morphology, being the grain sizes in the range of 0.1–0.5 µm (Fig. 6a and b). On the other hand, the vacuum-deposited film of the derivative **4**, with the long *N*-octyl chain, shows lower roughness and grains with a larger size around 0.5–1 µm with a terrace-like structure (Fig. 6c). The OTFT results are well correlated with the XRD and AFM studies. As deduced from GIXRD studies, the use of long alkyl chains induces a higher degree of long range organization of the molecules in the films, which is reflected on the larger grain size of the films (Fig. 6c), indicating larger crystalline domains.

Conclusions

The charge-transporting properties of a series of push-pull tricyanovinyl-substituted carbazole-based materials with different *N*-alkyl chain length have been evaluated. All compounds exhibited high thermal stability and a crystalline nature independently of the length of the alkyl chain. Absorption spectra of **1–5** were found to be identical in solution, but the maximum absorption peaks of **1–5** differed considerably in the thin films, pointing to the influence of the *N*-alkyl chain length on the molecular packing in the solid state. All compounds underwent facile reduction and showed identical EA values of 4.39 eV, which are appropriate for n-channel conduction. Similar electron mobilities in the range of 9×10^{-6} to 5×10^{-5} $cm^2\ V^{-1}\ s^{-1}$ were achieved for OTFT devices based on compounds **1–5**. The XRD study revealed that all compounds show a layered organization with an antiparallel arrangement and similar minimum interlayer distances (3.28–3.40 Å). Remarkably, the *N*-alkyl chain length governs the molecular arrangement in the solid state. Molecules with the shorter alkyl chains, from methyl to butyl, adopt a herringbone packing motif, in contrast to the coplanar one shown by molecules with longer alkyl chains, octyl and dodecyl. The strategy of introducing alkyl chains longer than 8 carbon units in the π-conjugated core generates segregated zones that contribute to the enhancement of the device performance.

Experimental

Materials

All chemicals were of commercial grade and used as received. 9-Methyl-9*H*-carbazole, 9-butyl-9*H*-carbazole, 9-octyl-9*H*-carbazole and 9-dodecyl-9*H*-carbazole were prepared following the procedures reported in the literature.[13–15] 9-Methyl-3-(1,2,2-tricyanovinyl)-9*H*-carbazole[10,16] (**1**), 9-ethyl-3-(1,2,2-tricyanovinyl)-9*H*-carbazole[16,17] (**2**) and 9-butyl-3-(1,2,2-tricyanovinyl)-9*H*-carbazole[16] (**3**) were prepared as described in the literature.

Synthesis of 9-octyl-3-(1,2,2-tricyanovinyl)-9*H*-carbazole (4)

9-Octyl-9*H*-carbazole (481 mg, 1.72 mmol) was dissolved in 10 mL of anhydrous DMF under a nitrogen atmosphere. Then, tetracyanoethylene (264 mg, 2.06 mmol) was added and the solution was stirred at 50 °C for 72 h. The cooled mixture was poured into a water/ice solution and the product was extracted with ethyl acetate. The organic layer was dried over Na_2SO_4, filtered off and the solvent was distilled off under reduced pressure. The crude was purified by flash column chromatography using first hexane followed by a mixture of hexane and ethyl acetate (from 10:1 to 2:1 v/v) as the eluent to give compound **4** as a red solid (272 mg; 42%). ^{1}H NMR (400 MHz, $CDCl_3$): δ = 8.82 (d, *J* = 2.0 Hz, 1H), 8.26 (dd, *J* = 9.0 Hz, *J* = 2.0 Hz, 1H), 8.16 (d, *J* = 7.8 Hz, 1H), 7.63–7.58 (m, 1H), 7.51 (d, *J* = 9.0 Hz, 1H), 7.50 (d, *J* = 8.2 Hz, 1H), 7.42–7.38 (m, 1H), 4.35 (t, *J* = 7.2 Hz, 2H), 1.94–1.87 (m, 2H), 1.42–1.20 (m, 10H), 0.86 (t, *J* = 6.8 Hz, 3H) ppm. ^{13}C NMR (100 MHz, $CDCl_3$): δ = 144.7, 141.6, 140.9, 128.2, 127.5, 124.4, 124.3, 122.7, 122.0, 121.4, 120.1, 114.6, 113.2, 112.8, 110.3, 110.3, 84.5, 44.0, 31.9, 29.4, 29.2, 29.1, 27.4, 22.7, 14.2 ppm. HRMS (ESI-MS): *m/z*: calcd for $C_{25}H_{28}N_5$: 398.2339 $(M + NH_4)^+$; found: 398.2340.

Synthesis of 9-dodecyl-3-(1,2,2-tricyanovinyl)-9*H*-carbazole (5)

9-Dodecyl-9*H*-carbazole (671 mg, 2.00 mmol) was dissolved in 10 mL of anhydrous DMF under a nitrogen atmosphere. Then, tetracyanoethylene (307 mg, 2.40 mmol) was added and the solution was stirred at 50 °C for 72 h. The cooled mixture was poured into a water/ice solution and the product was extracted with ethyl acetate. The organic layer was dried over Na_2SO_4, filtered off and the solvent was distilled off under reduced pressure. The crude was purified by flash column chromatography using first hexane followed by a mixture of hexane and ethyl acetate (from 10:1 to 5:1 v/v) as the eluent to give compound **5** as a red solid (409 mg; 47%). ^{1}H NMR (400 MHz, $CDCl_3$): δ = 8.82 (d, *J* = 2.1 Hz, 1H), 8.26 (dd, *J* = 9.0 Hz, *J* = 2.1 Hz, 1H), 8.16 (d, *J* = 7.8 Hz, 1H), 7.63–7.58 (m, 1H), 7.51 (d, *J* = 9.0 Hz, 1H), 7.49 (d, *J* = 8.2 Hz, 1H), 7.42–7.38 (m, 1H), 4.35 (t, *J* = 7.2 Hz, 2H), 1.94–1.87 (m, 2H), 1.42–1.20 (m, 18H), 0.88 (t, *J* = 6.9 Hz, 3H) ppm. ^{13}C NMR (100 MHz, $CDCl_3$): δ = 144.7, 141.6, 140.9, 128.2, 127.5, 124.4, 124.3, 122.6, 122.0, 121.4, 120.0, 114.6, 113.2, 112.8, 110.3, 110.3, 84.5, 44.0, 32.0, 29.7, 29.6, 29.6, 29.5,

View Article Online
DOI: 10.1039/C7CP05135B

29.4, 29.1, 27.4, 22.8, 14.3 ppm. HRMS (ESI-MS): *m/z*: calcd for $C_{29}H_{36}N_5$: 454.2965 $(M + NH_4)^+$; found: 454.2957.

Instrumentation and methods

Silica gel (SDS, 230–240 mesh) was used for flash column chromatography. ^{1}H NMR (400 MHz) and ^{13}C NMR (100 MHz) were collected on a Varian Mercury instrument. NMR spectra were processed using the MestReNova software. Chemical shifts were determined by taking the signal of the solvent as the reference. High-resolution mass spectrometry (HRMS) was performed on a LC/MSD-TOF Agilent Technologies apparatus by means of the electrospray (ESI-MS) technique. Single-crystal analyses were performed on a D8 Venture System equipped with a multilayer monochromator and a Cu microfocus (λ = 1.54178 Å) for compound **2** and a Mo microfocus (λ = 0.71073 Å) for compounds **3**–**5**. The frames were integrated using the Bruker SAINT software package using a narrow-frame algorithm. For **2** and **3**, the structure was solved using the Bruker SHELXTL Software Package and refined using SHELXL.[20] For **4** and **5**, the structure was solved and refined using the Bruker SHELXTL Software Package. CCDC 1562615 (**2**), CCDC 1562616 (**3**), CCDC 1562621 (**4**) and CCDC 1562623 (**5**). Thermogravimetric analyses (TGA) were performed on a TA Instruments Q50 at a heating rate of 20 °C min^{-1} under a nitrogen atmosphere. Differential scanning calorimetry (DSC) measurements were recorded on a TA Instruments Q2000 calorimeter at a scan rate of 10 °C min^{-1} under nitrogen atmosphere. UV-vis spectra were registered in a Varian Cary UV-Vis-NIR 500E spectrophotometer. Cyclic voltammograms were recorded on a microcomputer-controlled potentiostat/ galvanostat Autolab with PGSTAT30 equipment and GPES software. A cylindrical three-electrode cell was used. The reference electrode was a Ag/Ag$^+$ electrode (0.01 M $AgNO_3$ in acetonitrile). The counter and working electrodes were a platinum wire and a glassy-carbon electrode, respectively. All voltammetric curves were recorded under quiescent conditions, at a scan rate of 100 mV s^{-1} and under an argon atmosphere. All solutions were prepared in dichloromethane (1 mM) and tetrabutylammonium hexafluorophosphate (0.1 M) was used as the supporting electrolyte. The ionization potential (IP) and electron affinity (EA) values were estimated from the onset of the first oxidation and reduction peaks, respectively, as IP = $E^{ox}_{onset\ vs.\ Fc^+/Fc}$ + 5.39 and EA = $E^{red}_{onset\ vs.\ Fc^+/Fc}$ + 5.39, where –5.39 eV corresponds to the formal potential of the Fc^+/Fc couple in the Fermi scale.[21] Powder X-ray diffraction (XRD) measurements were obtained by using a PANalytical X'Pert PRO MPD θ/θ powder diffractometer of 240 millimetres of radius, in a configuration of convergent beam with a focalizing mirror and transmission geometry with a spinner glass capillary sample holder, a PIXcel detector, with Cu Kα radiation (λ = 1.5418 Å) and work power at 45 kV and 40 mA. Samples were prepared by introduction of the powder materials in *Lindemann* glass capillaries of 0.7 millimetres of diameter. GIXRD measurements of the vacuum-evaporated thin films of the organic materials (75 nm) were performed in a PANalytical X'Pert PRO MRD diffractometer with a PIXcel detector, a parabolic Göbel mirror at the incident beam and a parallel plate collimator at the diffracted beam, with Cu Kα radiation (λ = 1.5418 Å) and work power at 45 kV and 40 mA. The angle of incidence used was ω ~0.2°. AFM experiments were conducted using an AFM Multimode 8 system attached to a Nanoscope V electronic unit (Bruker).

OTFT fabrication and measurements

OTFT devices were fabricated using the bottom-gate top-contact geometry. The substrate consisted in a thermally oxidized crystalline silicon wafer that provided a gate dielectric (SiO_2) of thickness 110 nm. The SiO_2 surface was treated with either polystyrene (PS) or octadecyltrichlorosilane (OTS). For the deposition of the PS layer, a solution of PS in toluene (4 mg mL^{-1}) was deposited drop wise on the substrate. The substrate was spun at 500 rpm for 5 s and 2500 rpm for 30 s with a P6700 spin coater. For OTS SAM fabrication,[22] the substrates were immersed in a 2 mM toluene solution of OTS for 24 hours at room temperature. Then, the substrates were cleaned by ultrasonic treatment in toluene, acetone and isopropyl alcohol, and subsequently dried by a nitrogen blow and heated at 100 °C for 10 minutes. Organic materials were deposited by thermal evaporation in a vacuum system with a base pressure below 10^{-6} mbar. The sublimation temperature for the organic compounds was regulated to maintain a stable deposition rate around 0.1–0.2 Å s^{-1} to obtain around 75 nm thickness layers. Then, the samples were transferred to a different vacuum chamber to evaporate the metallic contacts. Gold was used for drain and source electrodes, which were defined using a metallic mask that defines a channel length (L) and width (W) of 80 µm and 2 mm, respectively. The fabricated OTFTs were electrically characterized in the dark and under vacuum conditions. The electrical characteristics were measured using a Keithley 2636A source meter. The charge carrier mobility (μ) in the saturated region and the threshold voltage (V_{th}) were calculated from eqn (1):

$$I_D = \frac{WC_{ox}\mu}{2L}(V_G - V_{th})^2 \quad (1)$$

where W and L are the channel width and length, respectively, and C_{ox} is the unit dimensional dielectric capacitance of gate insulator.

Acknowledgements

Financial support from the Ministerio de Economía y Competitividad (CTQ2015-65770-P MINECO/FEDER and ENE2014-56237-C4) is gratefully acknowledged.

Notes and references

1 a) Y. Yamaguchi, M. Takubo, K. Ogawa, K.-I. Nakayama, T. Koganezawa and H. Katagiri, *J. Am. Chem. Soc.*, 2016, **138**, 11335; b) M. Mamada, H. Shima, Y. Yoneda, T. Shimano, N. Yamada, K. Kakita, T. Machida, Y. Tanaka, S. Aotsuka, D. Kumaki and S. Tokito, *Chem. Mater.*, 2015, **27**, 141.
2 a) K.-H. Kim, S.-J. Yoo and J.-J. Kim, *Chem. Mater.*, 2016, **28**, 1936; b) M. Zhu and C. Yang, *Chem. Soc. Rev.*, 2013, **42**, 4963.

View Article Online
DOI: 10.1039/C7CP05135B

3 L. Dou, J. You, Z. Hong, Z. Xu, G. Li, R. A. Street and Y. Yang, *Adv. Mater.*, 2013, **25**, 6642.
4 a) X. Gao and Y. Hu, *J. Mater. Chem. C*, 2014, **2**, 3099; b) Y. Zhao, Y. Guo and Y. Liu, *Adv. Mater.*, 2013, **25**, 5372.
5 C. R. Newman, C. D. Frisbie, D. A. S. Filho, J.-L. Bredas, P. C. Ewbank and K. R. Mann, *Chem. Mater.*, 2004, **16**, 4436.
6 J. Mei, Y. Diao, A. L. Appleton, L. Fang and Z. Bao, *J. Am. Chem. Soc.*, 2013, **135**, 6724.
7 a) B. Kang, F. Ge, L. Qiu and K. Cho, *Adv. Electron. Mater.*, 2017, **3**, 1600240; b) T. Lei, J.-Y. Wang and J. Pei, *Chem. Mater.*, 2014, **26**, 594; c) J. Mei and Z. Bao, *Chem. Mater.*, 2014, **26**, 604.
8 a) M. Reig, J. Puigdollers and D. Velasco, *J. Mater. Chem. C*, 2015, **3**, 506; b) C. Xiao, W. Jiang, X. Li, L. Hao, C. Liu and Z. Wang, *ACS Appl. Mater. Interfaces*, 2014, **6**, 18098; c) H. Zhao, L. Jiang, H. Dong, H. Li, W. Hu and B. S. Ong, *ChemPhysChem*, 2009, **10**, 2345.
9 a) C.-H. Lee, Y.-Y. Lai, J.-Y. Hsu, P.-K. Huang and Y.-J. Cheng, *Chem. Sci.*, 2017, **8**, 2942; b) M.-H. Lee, J. Kim, M. Kang, J. Kim, B. Kang, H. Hwang, K. Cho and D.-Y. Kim, *ACS Appl. Mater. Interfaces*, 2017, **9**, 2758; c) J. Y. Back, T. K. An, Y. R. Cheon, H. Cha, J. Jang, Y. Kim, Y. Baek, D. S. Chung, S.-K. Kwon, C. E. Park and Y.-H. Kim, *ACS Appl. Mater. Interfaces*, 2015, **7**, 351; d) H. B. Akkerman, S. C. B. Mannsfeld, A. P. Kaushik, E. Verploegen, L. Burnier, A. P. Zoombelt, J. D. Staathoff, S. Hong, S. Atahan-Evrenk, X. Liu, A. Aspuru-Guzik, M. F. Toney, P. Clancy and Z. Bao, *J. Am. Chem. Soc.*, 2013, **135**, 11006.
10 M. Reig, G. Bagdziunas, D. Volyniuk, J. V. Grazulevicius and D. Velasco, *Phys. Chem. Chem. Phys.*, 2017, **19**, 6721.
11 a) M. Reig, C. Gozálvez, R. Bujaldón, G. Bagdziunas, K. Ivaniuk, N. Kostiv, D. Volyniuk, J. V. Grazulevicius and D. Velasco, *Dyes Pigm.*, 2017, **137**, 24; b) B. R. Kaafarani, A. O. El-Ballouli, R. Trattnig, A. Fonari, S. Sax, B. Wex, C. Risko, R. S. Khnayzer, S. Barlow, D. Patra, T. V. Timofeeva, E. J. W. List, J.-L. Brédas and S. R. Marder, *J. Mater. Chem. C*, 2013, **1**, 1638; c) J.-F. Morin, M. Leclerc, D. Adès and A. Siove, *Macromol. Rapid. Commun.*, 2005, **26**, 761.
12 J. L. Díaz, A. Dobarro, B. Villacampa and D. Velasco, *Chem. Mater.*, 2001, **13**, 2528.
13 G. Li, X. Zhou, P. Yang, Y. Jian, T. Deng, H. Shen and Y. Bao, *Tetrahedron Lett.*, 2014, **55**, 7054.
14 Y. Zou, M. Wan, G. Sang, M. Ye and Y. Li, *Adv. Funct. Mater.*, 2008, **18**, 2724.
15 L. Schweighauser and H. A. Wegner, *Chem. Commun.*, 2013, **49**, 4397.
16 S. Banerjee, F. Ali, P. K. Nayak and N. Agarwal, *Thin Solid Films*, 2012, **520**, 2644.
17 J. E. Kuder, W. W. Limburg, J. M. Pochan and D. Wychick, *J. Chem. Soc., Perkin Trans. 2*, 1977, 1643.
18 E. G. Popova, L. A. Chetkina and B. V. Kotov, *Zh. Strukt. Khim.*, 1981, **22**, 116.
19 a) S. Hüttner, M. Sommer and M. Thelakkat, *Appl. Phys. Lett.*, 2008, **92**, 093302; b) C. Müller, S. Goffri, D. W. Breiby, J. W. Andreasen, H. D. Chanzy, R. A. J. Janssen, M. M. Nielsen, C. P. Radano, H. Sirringhaus, P. Smith and N. Stingelin-Stutzmann, *Adv. Funct. Mater.*, 2007, **17**, 2674.
20 G. M. Sheldrick, *Acta Crystallogr.*, 2008, **A64**, 112.
21 a) C. M. Cardona, W. Li, A. E. Kaifer, D. Stockdale and G. C. Bazan, *Adv. Mater.*, 2011, **23**, 2367; b) A. J. Bard and L. R. Faulkner, *Electrochemical Methods: Fundamentals and Applications*, WILEY-VCH, New York, 2001.
22 a) A. Ghalgaoui, R. Shimizu, S. Hosseinpour, R. Álvarez-Asencio, C. McKee, C. M. Johnson and M. W. Rutland, *Langmuir*, 2014, **30**, 3075; b) D. Song, H. Wang, F. Zhu, J. Yang, H. Tian, Y. Geng and D. Yan, *Adv. Mater.*, 2008, **20**, 2142.

View Article Online
DOI: 10.1039/C7CP05135B

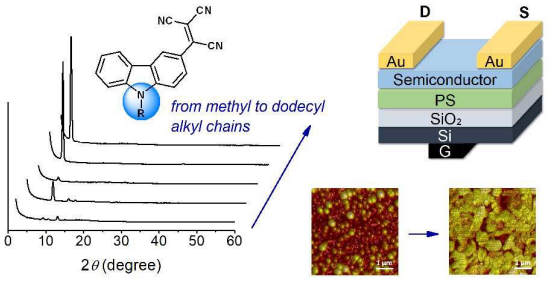

n-Type Organic Thin-Film Transistors (OTFTs) were fabricated and characterised from a series of tricyanovinyl-substituted carbazole-based materials as the active layer. The effect of the *N*-alkyl chain length of the carbazole moiety on the charge-transporting properties is here evaluated. X-Ray diffraction (XRD) studies gave insights into the main intermolecular interactions, molecular packing motif and degree of molecular order in the thin films that justified the performance of the devices.